Hydrogen Sulfide (H_2S) Sensor: A Concept of Physical Versus Virtual Sensing

Ahmed Alsarraj, Atiq ur Rehman, *Member, IEEE*, Samir Brahim Belhaouari, *Senior Member, IEEE*, Khaled M. Saoud, and Amine Bermak, *Fellow, IEEE*

***Abstract*— Hydrogen sulfide (H_2S) presents many hazardous traits such as corrosive, explosive, toxic, and flammable. It is slightly denser than air, and a mixture of H_2S and air can be volatile. Therefore, a reliable and robust measurement system is required to effectively detect and quantify H_2S in many applications, such as oil and gas industries. There are several methods available in the literature to quantify H_2S in fuel gases; however, only a few are available in case of air samples. Furthermore, array-based sensors are more reliable in the detection of volatile organic compounds (VOCs); however, sensor arrays are more expensive and challenging to produce. To overcome the limitations of producing physical sensor arrays, this article proposes a concept of virtual sensing that enables to augment a single sensing platform into a virtual array, thus, increasing the detection accuracy at no extra cost of producing a large physical sensors array. The merits of the proposed system are as follows: 1) a virtual sensing concept is combined with a physical sensing platform to enhance the proposed model's estimation power in quantifying H_2S in air samples; 2) a new feature extraction method based on fractional derivatives is proposed to further enhance the model's learning capabilities; 3) an array of four gas sensors is fabricated in the in-house foundry to record and analyze the signature of H_2S at various concentration levels; 4) a shallow neural network (NN) model is trained and tested on the recorded data, and based on the NN's input–output relation, a mathematical model is presented for the quantification of H_2S; and 5) the proposed model is a highly sensitive and reliable H_2S gas sensing scheme with the ability to detect the gas instantaneously. The proposed gas quantification model has the advantages of being low cost, easy to implement, and fast operation compared with the analytical solutions. Furthermore, it is extensively tested and validated using real gas data.**

***Index Terms*— Electronic nose, gas estimation, mathematical modeling, neural networks (NNs), sensors, virtual sensing.**

Manuscript received June 24, 2021; revised September 19, 2021; accepted October 1, 2021. Date of publication October 26, 2021; date of current version November 9, 2021. This work was supported in part by the National Priorities Research Program (NPRP) from the Qatar National Research Fund (a member of Qatar Foundation) under Grant NPRP10-0201-170315 and Grant NPRP11S-0110-180246 and in part by Qatar National Library (QNL) for supporting the publication charges of this article. The Associate Editor coordinating the review process was Rajarshi Gupta. *(Corresponding author: Atiq ur Rehman.)*

Ahmed Alsarraj is with the Sustainability Division, College of Science and Engineering, Hamad Bin Khalifa University, Doha, Qatar (e-mail: aalsarraj@hbku.edu.qa).

Atiq ur Rehman, Samir Brahim Belhaouari, and Amine Bermak are with the ICT Division, College of Science and Engineering, Hamad Bin Khalifa University, Doha, Qatar (e-mail: atrehman2@hbku.edu.qa; sbelhaouari@hbku.edu.qa; abermak@hbku.edu.qa).

Khaled M. Saoud is with Liberal Arts and Science Program, Virginia Commonwealth University in Doha, Doha, Qatar (e-mail: s2kmsaou@vcu.edu).

Digital Object Identifier 10.1109/TIM.2021.3120150

I. Introduction

HYDROGEN sulfide (H_2S) is a highly toxic colorless gas which possesses a characteristic odor of rotten eggs. Health effects due to the exposure of H_2S remain negative in the majority of the well-documented studies, especially if the levels of H_2S are above 1 ppm in air [1]. The human nervous system and the respiratory tract remain most sensitive to the exposure of H_2S. Although the odor of H_2S becomes detectable at 0.0005 ppm by a human nose, at higher concentrations (100 ppm), the sense of smell is lost after an exposure of 2–15 min [2]. Therefore, the odor of gas remains an ineffective warning toward the presence and detection of the respective gas.

Gas chromatography (GC)-based methods have been frequently employed to monitor the presence of H_2S in different scenarios with high precision [3]–[5]. However, the applicability of these methods in real scenarios, especially in environmental monitoring, is not very simple and requires a multistage protocol starting from sampling till the final quantification [6]. Besides chromatography [GC/high performance liquid chromatography (HPLC)], there exist a variety of other analytical approaches for the detection of H_2S. These approaches include fluorimetry and colorimetry, electrochemistry, and inductively coupled plasma-optical emission spectroscopy (ICP-OES) [7]–[14]. Among these, GC and ICP-OES also perform a nonstatic type of detection and require a tedious procedure of sample pretreatment, and incur high cost [15], [16]. Besides these analytical approaches, there are studies based on optical approaches [17]–[19] and nanoparticle sensors [20]–[22]. Although these approaches exhibit high sensitivity, the opaque solution of metrices and colored interferents limit their detection accuracy [15].

In comparison with approaches based on chromatography, optical, and acoustic gas sensing, electrochemical gas sensing has remained popular due to: 1) being more inexpensive as compared with others; 2) high selectivity and reproducibility; 3) low energy linear output; and 4) ppm-level detection with high accuracy [23]. However, electrochemical sensors have a low shelf life and remain highly sensitive to temperature fluctuations [24].

Mostly used chemical sensors for monitoring harmful pollutants in real time are either electrochemical sensors [25], metal-oxide semiconducting sensors [26]–[29], optical sensors [30], piezoelectric sensors [31], or sensors' array [32], [33]. These sensor-based devices have several advantages, such as low cost, high sensitivity, easy operation,

and fast response [6]. Among these, metal oxide gas sensors have demonstrated a capability to detect more than 150 gases with an added advantage of low cost, ease of use, portability, compact size, low power consumption, and high sensitivity [34]. A complete review on the recent advances and use of metal oxide gas sensors for the detection of H_2S is provided in [34]. In terms of sensing H_2S using a metal-oxide sensor, the most important material is an n-type WO_3 due to its structural simplicity, high sensitivity, and low cost, especially in nano-size structures [35]. Moreover, there are studies in existing literature suggesting that the Ag-doped WO_3 has better sensing performance and shorter recovery time as compared with the pure WO_3 sensor [36]–[38].

Furthermore, an approach known as *smart gas sensing* combines a sensing array with a machine learning model. This combination enhances the prediction accuracy of the system [39]. There are several existing studies based on smart sensing incorporating artificial intelligence/machine learning models for enhancing the prediction accuracy of the system for quantification and identification of gases [40]–[42]. Electronic noses are devices built on the concept of *smart sensing* for various applications, including the monitoring of toxic gases [43], [44]. Although, these systems require training data to train the ML model, but once the model is trained, the system can predict and quantify the gases with high accuracy. Furthermore, these systems have already demonstrated robustness against the sensors' long-term drift problem, which makes them feasible for long-term real operations [45], [46].

Keeping in view the demonstrated advantages of electronic nose systems, metal oxide gas sensors, and limitations of producing large sensor arrays, this work proposes a system based on the concept of *virtual sensing*, which enables to augment a single sensing platform into a virtual array, and thus increases the prediction accuracy of the system. In order to build a virtual sensors array, an array of four physical gas sensors is used and is operated at four different temperatures. By operating the four sensors array at four different temperatures, a virtual response of 16 sensors array is recorded and analyzed for estimation of H_2S in air samples. The four sensors array is built in the in-house foundry using tungsten oxide (WO_3) and silver with different weight percentages (0%, 1%, 3%, and 5%). The virtual sensors array is used to acquire different signatures of H_2S at different concentration values. The collected data are used to define a mathematical model based on the input–output relation of a shallow NN, and to further enhance the estimation performance of the proposed model, a new set of fractional derivative features (FDFs) are proposed. The newly proposed feature extraction scheme is based on fractional calculus, which is a branch of calculus that generalizes the differentiation and integration to a fundamental noninteger-order operator. Thus, it enables to provide a better realization of complex systems where details provided by integer order operator are not sufficient. The newly proposed FDF extraction scheme has enabled to significantly improve the performance of the overall system in terms of estimating the concentration of H_2S in air samples.

After extensive experimentation, some useful recommendations are drawn from the study to quantify H_2S in different scenarios. A comparison of performance based on actual versus virtual sensors and a comparison based on the performance of actual response versus the proposed FDFs is provided in detail, highlighting the benefits and limitations of the proposed system.

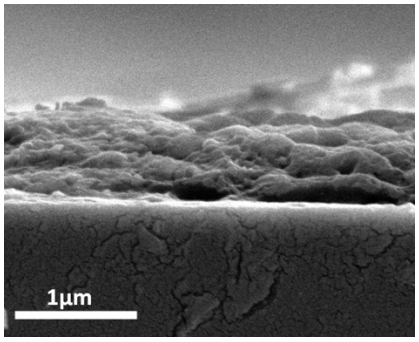

Fig. 1. Cross-sectional SEM image of 3% Ag/WO_3 thin film deposited on silicon substrate.

The rest of this article is organized as follows. Section II (Experimental Setup), Section III (Methodology), Section IV (Performance Evaluation), and Section V (Conclusion).

II. Experimental Setup

A. Sensor Fabrication

Gold interdigitated electrodes (IDEs) with a gap of 200 μm between the electrodes are used to fabricate the sensor. A platinum heating layer on the back of the electrodes is used to control the temperature through the highly conductive ceramic substrate. Two 5-cm-long wires were soldered on the electrodes to perform electrical measurements. For creating a homogeneously deposited layer on the gold IDE, an ultrasonic spray pyrolysis machine is used to spray the electrodes with a mixed solution of tungsten oxide (WO_3) and silver with different weight percentages (0%, 1%, 3%, and 5%). The uniformity of the layer is controlled by using an ultrasonic spray pyrolysis machine for deposition of the material. The method used ensures that the thickness is from few nanometers to micrometers by adjusting the number of deposition cycles. Fig. 1 shows the scanning electron microscope (SEM) cross section image of the surface of 3% Ag/WO_3 thin film with 15 deposition cycles. The thickness of the thin film was on average between 1 and 2 μm.

To control the moisture effect, a flow of zero (dry) air was flushed into the gas testing chamber which contains the sensor. This was done before and after each gas testing to ensure that the effect of humidity was minimum. The gas is diluted with the same synthesized pure dry air with 99.999%, and this ensures the elimination of moisture. Moreover, the gas generator device is provided with moisture traps that eliminate any moisture. Another experiment was done where humidity was introduced inside the gas testing chamber.

To study the tungsten oxide doped silver (Ag/WO_3) microstructure, transmission electron microscope (TEM) was used to explore the variations in the nanoparticles of tungsten and to detect the presence of Ag species. TEM micrographs of tungsten oxide-doped silver oxide (Ag/WO_3) are shown in Fig. 2. The micrographs show that there are sheet-like

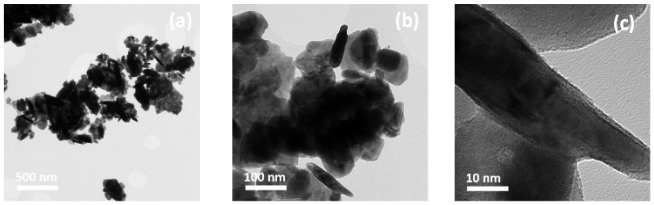

Fig. 2. TEM micrograph of Ag/WO_3 nanoparticles with different scales. (a) 500 nm. (b) 100 nm. (c) 10 nm.

nanoparticles of WO_3 with sizes varying from 20 to 60 nm. The particles are agglomerated together and exist in coalescences of nanosheets. The Ag nanoparticles are well dispersed on the edges of the surface of the WO_3 particles in sizes that vary between 5 and 15 nm, as can be seen in Fig. 2(c).

B. Data Acquisition System

The sensor is mounted inside a testing chamber that encompasses a heating plate for temperature control of the sensor. A gas generator (Dynacalibrator VICI 340) that includes a permeation tube with concentrated gas (a liquid phase of H_2S) is used to generate precise gas concentrations. The concentration is controlled by varying the temperature and dilution gas flow, which is supplied from the synthetic air cylinder. It generates gas vapor from heating a permeation tube, and the concentration is controlled by changing the diluting airflow. To measure the concentration, a mathematical equation is provided in the user manual of VICI 340 Dynacalibrator. Keithley 2450 source meter is used to obtain the voltage and current variations in the sensor signal due to gas exposure, and the data are transferred and analyzed through a computer. The sampling rate to store the response is kept at 600 samples/min, and a normalized response is recorded as

$$R = \left|\frac{\Delta I}{I_A}\right|, \quad \Delta I = I_G - I_A \tag{1}$$

where I_G is the current flow recorded when the gas is exposed to the sensor, I_A is the current flow recorded on the exposure of dry air, and ΔI represents the change in response of the sensor. The response of sensors is recorded at four varying temperatures (T = 25 °C, 80 °C, 150 °C, 200 °C). This occurs due to the fact that upon exposure to ambient air, the nanomaterial absorbs oxygen on its surface by capturing free electrons. This creates a depletion region on the surface of oxidized material which affects the conductivity of the sensor and varies with operating temperature. Due to this change in conductivity of the sensor, operating the sensor at different temperatures provides different responses toward the concentration of H_2S. Therefore, the combined change in response by different sensors operating at different temperatures can be used as a unique signature by a pattern recognition algorithm to estimate different concentration levels of H_2S. Fig. 3 provides an overview of the experimental setup and the in-house fabricated gas sensors.

III. Methodology

The proposed methodology is based on a virtual sensing concept which employs a shallow NN model to quantify H_2S in air samples. The performance of the model is further enhanced by proposing new FDFs. The details of the proposed model are given below:

A. Feature Extraction

Features play a vital role in the recognition accuracy of a machine/deep learning model. The state-of-the-art feature extraction and selection methods like principal component analysis (PCA), linear discriminant analysis (LDA), and particle swarm optimization (PSO) have been successfully used in the literature for gas identification and quantification [47]–[50]. In order to effectively utilize a neural network (NN) for the estimation of H_2S, a new set of features based on the fractional derivatives is proposed for learning an NN in this study.

Fractional order differential equations are generalized noninteger-order differential equations that may be generated in time and space using the nonlocal relationships' power law memory kernel. They are a useful tool for describing the memory of various substances as well as the nature of heredity. A noninteger differentiation/integration operator is used in fractional calculus to investigate various possible ways of defining real number powers or complex number powers of the operator. Based on the real number powers of the differentiation operator, the fractional derivative models are able to provide details that are not provided by the integer-type operator or by other linear transformation methods. PCA (unsupervised method) and LDA (supervised method), on the other hand, are both linear transformation methods that decompose matrices of eigenvalues and eigenvectors. Compared with PCA and LDA, FDFs have shown significant performance in terms of estimation of H_2S in air samples.

For fractional calculus, suppose a noninteger-order operator ${}_a\mathcal{D}_t^\alpha$, where $\alpha \epsilon \mathbb{R}$ and the bounds of operation are a and t. A continuous ${}_a\mathcal{D}_t^\alpha$ operator can be defined as

$${}_a\mathcal{D}_t^\alpha = \begin{cases} \dfrac{d^\alpha}{dt^\alpha}, & \alpha > 0 \\ 1, & \alpha = 0 \\ \displaystyle\int_a^t (d\tau)^\alpha, & \alpha < 0. \end{cases} \tag{2}$$

The most commonly used definition of general differ-integral is Grünwald–Letnikov [51], defined as

$${}_a\mathcal{D}_t^\alpha f(t) = \lim_{h\to 0} h^{-\alpha} \sum_{j=0}^{\left[\frac{t-a}{h}\right]} (-1)^j \binom{\alpha}{j} f(t - jh). \tag{3}$$

For the calculation of fractional-order derivative, a relation derived from (3) can be used which is defined as

$$\begin{aligned} {}_{(k-\frac{L_m}{h})}\mathcal{D}_{t_k}^q f(t) &\approx h^{-q} \sum_{j=0}^{k} (-1)^j \binom{q}{j} f(t_k - j) \\ &= h^{-q} \sum_{j=0}^{k} c_j^{(q)} f(t_k - j) \end{aligned} \tag{4}$$

where $t_k = kh$, h is the time step, L_m is the "memory length," and $c_j^{(q)} (j = 0, 1, \ldots, k)$ are binomial coefficients calculated

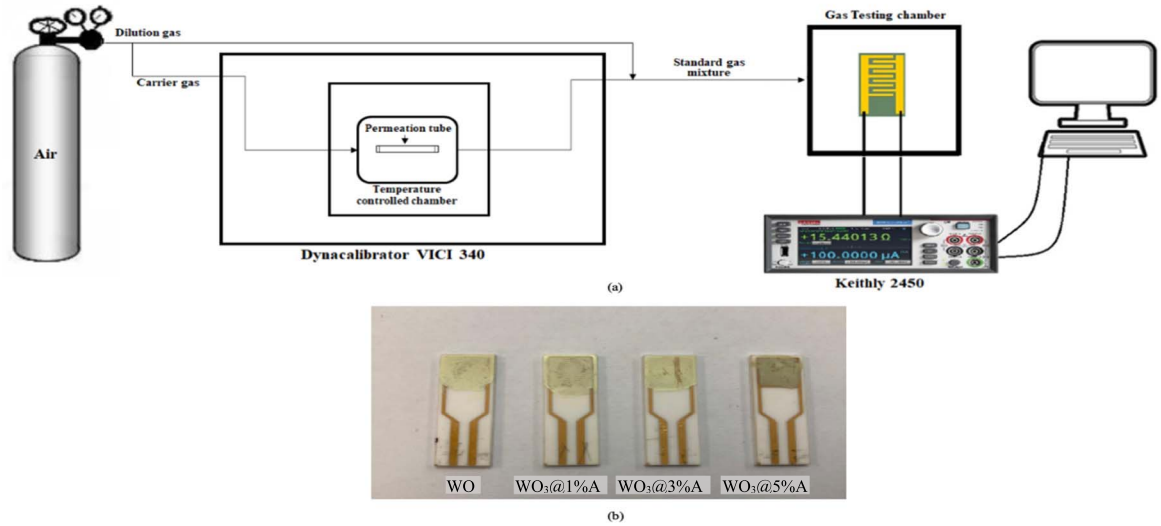

Fig. 3. Experimental setup. (a) Data acquisition system. (b) Sensors built in the inhouse foundry.

as

$$c_0^{(q)} = 1, \quad c_j^{(q)} = \left(1 - \frac{1+q}{j}\right) c_{j-1}^{(q)}. \tag{5}$$

The generalization of binomial coefficients to noninteger values can be made if the factorial is written as a *gamma* function [52]

$$(-1)^j \binom{q}{j} = (-1)^j \frac{\Gamma(q+1)}{\Gamma(j+1)\Gamma(q-j+1)} = \frac{\Gamma(j-q)}{\Gamma(-q)\Gamma(j+1)} \tag{6}$$

where Γ is the *gamma* function defined as

$$\Gamma(n) = (n-1)! \quad \forall n \epsilon \mathbb{R}. \tag{7}$$

The above Grünwald–Letnikov definition of fractional derivate is used to extract different features from the response curve of sensors and a feature vector is recorded. Ten values of fractional order derivative between $0 < \alpha < 1$ are used to extract the features for each sensor response. An array of four sensors is used to record the response at four different operating temperatures, and for each response, ten additional FDFs are extracted. MATLAB code to compute fractional derivatives using the above Grünwald–Letnikov definition and α values is given in [53].

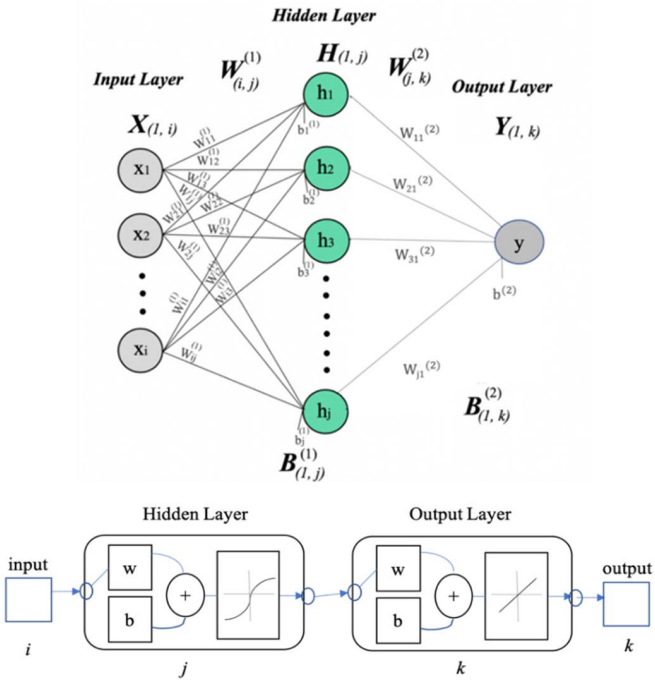

Fig. 4. Architecture of shallow NN used for mathematical modeling of H_2S concentration estimation, i represents the number of inputs, j represents the number of hidden neurons, and k represents the number of outputs.

B. Mathematical Model

The estimation of H_2S is mathematically modeled by employing a shallow NN model. Different experimentations were carried out by varying the number of neurons and layers of an NN and based on the performance of different architectures in terms of estimation accuracy and computational complexity, a shallow network of ten hidden neurons is recommended to derive a final mathematical model. Fig. 4 describes a general feedforward NN architecture used for mathematical modeling where i represents the number of inputs, j represents the number of hidden neurons, and k represents the number of outputs. In this case study, the value of $k = 1$ remains constant to estimate the concentration of H_2S.

Five different values of $j = 5, 10, 15, 20$, and 30 with one and two hidden layers were tested before finalizing the estimation model. The results for this experimentation using an array of four sensors array operating at 25 °C are provided in Table I and are visually analyzed in Fig. 5. From the results provided, it can be seen that the estimation accuracy of H_2S increases with an increase in the number of neurons and hidden layers. However, increasing the number of hidden layers and

TABLE I
NN SIMULATION RESULTS FOR FOUR SENSORS ARRAY OPERATING AT 25 °C WITH DIFFERENT NUMBER OF NEURONS AND HIDDEN LAYERS

	Single layer **5 neurons**	Single layer **10 neurons**	Single layer **15 neurons**	Single layer **20 neurons**	Single layer **30 neurons**
MSE	1622.52	993.85	749.61	709.10	682.10
R (Validation)	0.9159	0.9512	0.9627	0.9658	0.9686
R (Testing)	0.9138	0.9562	0.9600	0.9664	0.9723
R (Training)	0.9133	0.9582	0.9646	0.9667	0.9713
R (All)	0.9137	0.9569	0.9626	0.9665	0.9710
	Two layers 5 neurons each	**Two layers 10 neurons each**	**Two layers 15 neurons each**	**Two layers 20 neurons each**	**Two layers 30 neurons each**
MSE	803.65	553.73	478.82	453.24	451.48
R (Validation)	0.9477	0.9725	0.9772	0.9791	0.9781
R (Testing)	0.9392	0.9767	0.9745	0.9775	0.9853
R (Training)	0.9495	0.9751	0.9759	0.9808	0.9828
R (All)	0.9477	0.9750	0.9758	0.9800	0.9825

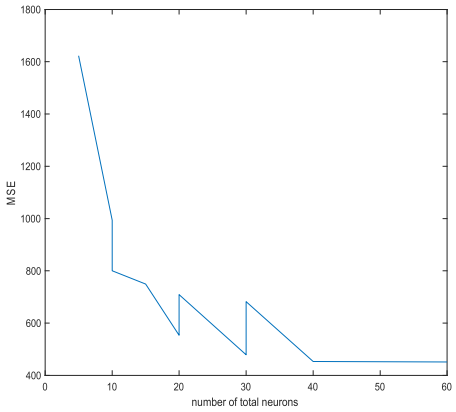

Fig. 5. Performance analysis with respect to an increase in number of neurons and hidden layers.

the number of neurons brings more computational complexity, thus requiring more computational resources. Therefore, to limit the number of hidden layers and the number of neurons, the concept of virtual sensing enhanced with FDFs is proposed. The proposed idea enables to limit the number of hidden neurons to ten with only one hidden layer making the proposed architecture computationally less expensive.

In the case of inputs, a comprehensive analysis is performed to evaluate different sensors, different sensors operating at different temperatures, and the combined effect of sensors as a special case of virtual sensing.

After extensive experimentation and testing, the following mathematical model is proposed for the estimation of H_2S in air samples:

$$y = \sum_{n=1}^{j} W_n^{(2)} \left(\text{tansig} \left(\sum_{m=1}^{i} W_m^{(1)} X_m + B_{1j}^{(1)} \right) \right) + B_{1k}^{(2)} \quad (8)$$

which can be further expanded as

$$y = \sum_{n=1}^{j} W_n^{(2)} \times \left(\frac{2}{1 + e^{-2 \times \sum_{m=1}^{i} W_m^{(1)} X_m + B_{1j}^{(1)}}} - 1 \right) + B_{1k}^{(2)} \quad (9)$$

where $W_n^{(2)}$ is the hidden layer weights, $W_m^{(1)}$ is the input layer weights, $B_{1k}^{(2)}$ is the output bias, $B_{1j}^{(1)}$ is the hidden layer biases,

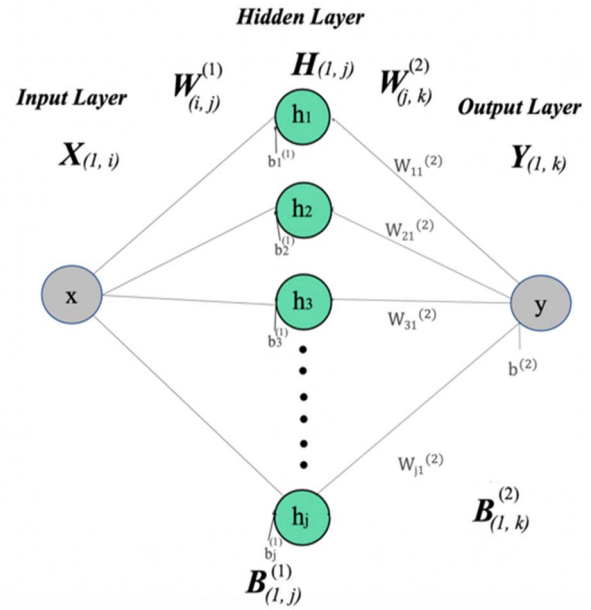

Fig. 6. Shallow NN architecture for a single sensor evaluation.

X_m is the input vector of length m, n is the number of hidden neurons, and y is the output representing the estimated value of H_2S.

IV. PERFORMANCE EVALUATION

The evaluation of the proposed system is performed in four different ways: 1) evaluation of a single sensor operating at different temperatures; 2) evaluation of four sensors array operating at different temperatures; 3) evaluation of proposed FDFs; and 4) evaluation of virtual sensors array. The sampling rate for data acquisition is kept at 600 samples/min, and the normalized response for 26 833 samples at seven different concentration levels is used for experimentation. The total data size for four different evaluations varies based on the evaluation. The data size for the evaluation of a single WO_3 sensor at four different temperatures is 26 833 × 4. The data size for the evaluation of four sensors array operating at four different temperatures is 26 833 × 16, whereas, for the evaluation with

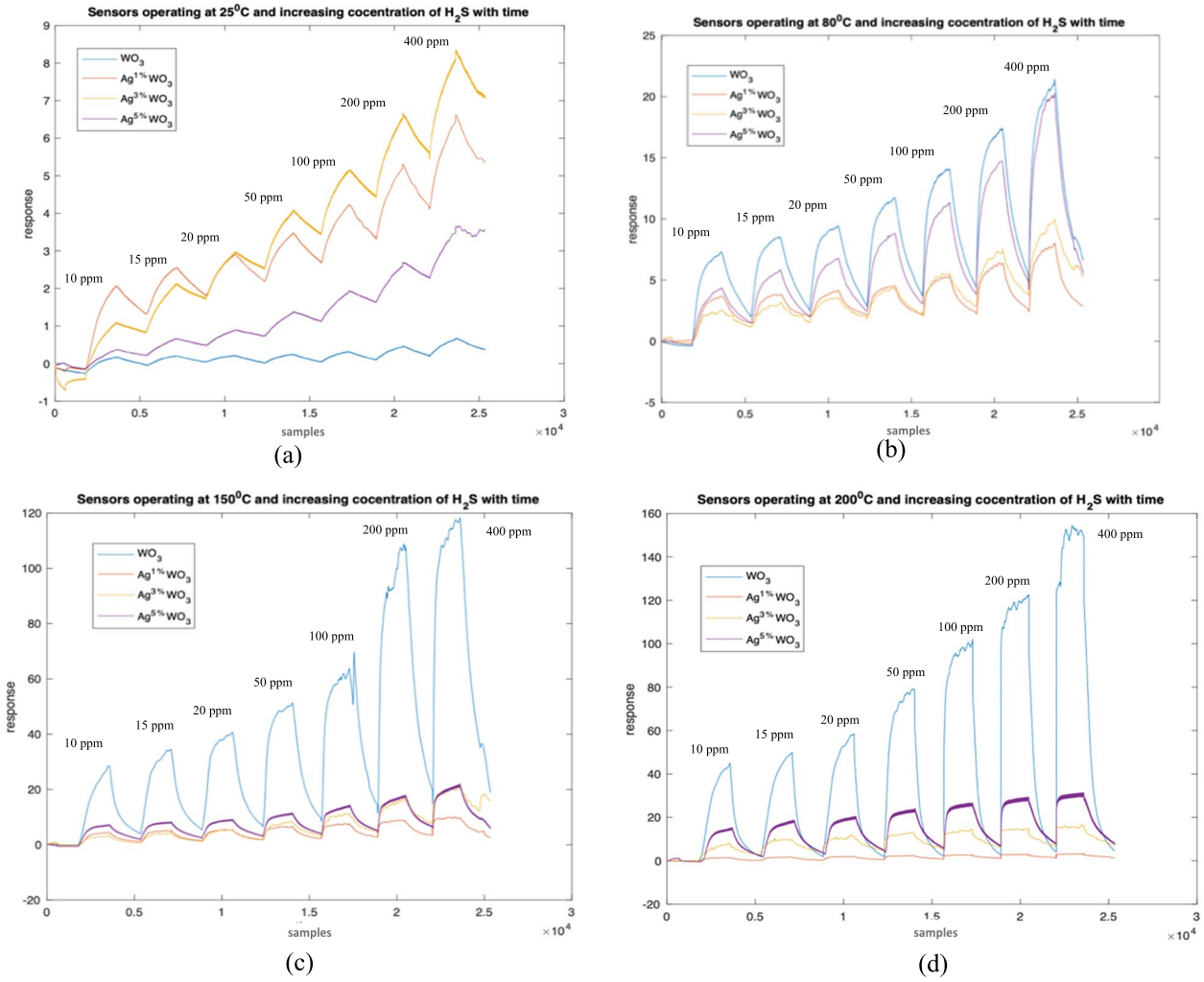

Fig. 7. Response of sensors toward seven different concentration levels of H_2S. Sensors operating at (a) 25 °C, (b) 80 °C, (c) 150 °C, and (d) 200 °C.

FDFs, ten extra features are calculated for each response variable which makes a maximum data size of 26 833 × 176. Out of these 176 response variables, 16 correspond to the 16 virtual sensors, whereas the remaining 160 correspond to the FDF features. All these evaluations are provided in detail, as follows.

A. Evaluation of a Single WO_3 Sensor Operating at Different Temperatures

The NN architecture employed for a single sensor evaluation is shown in Fig. 6. The architecture used for the evaluation of a sensor has the ability to estimate the concentration of H_2S at any given instance. The sensor's response is directly fed to the network and there is no requirement to wait until the steady-state response of the sensor. As soon as the network receives a response value from the sensor, it gives an estimation of the concentration of H_2S.

The actual response of individual sensors operating at different temperatures toward an increase in the concentration of H_2S is shown in Fig. 7(a–d). The concentration levels of H_2S exposed to the sensors are 10, 15, 20, 50, 100, 200, and 400 ppm. It can be seen from the response curves in Fig. 7 that

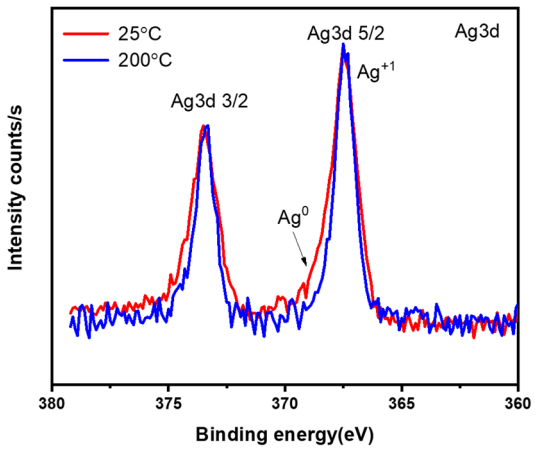

Fig. 8. Ag 3-D XPS spectra of Ag/WO_3 in room temperature (red) and when annealed to 200 °C (blue).

the WO_3 sensor has a low sensitivity toward the concentration of H_2S while operating at low temperatures. In contrast, the sensors doped with Ag remain more stable toward the change

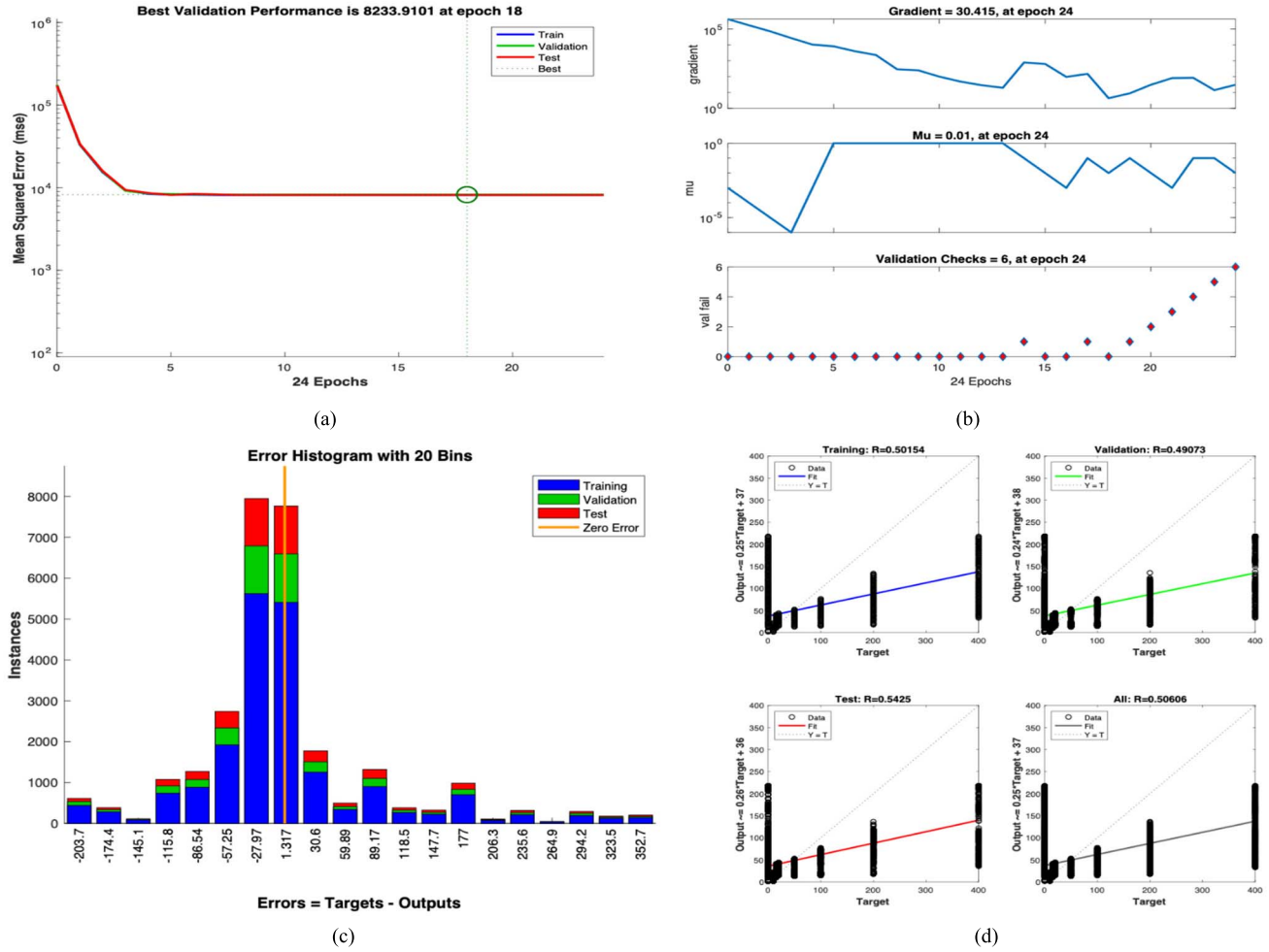

Fig. 9. Performance of a shallow NN for prediction of H_2S using a single WO_3 sensor operating at 25 °C. (a) Performance based on mean square error. (b) Training state and validation checks. (c) Error histogram. (d) Regression.

in operating temperature. Moreover, the response of Ag-doped sensors reduces at higher temperatures. This happens because Ag nanoparticles work as active catalytic sites that increase the conductivity of the material. The depletion layer width is reduced when Ag is added to WO_3 due to the transfer of electrons from Ag. However, at higher temperatures, the rate of oxidation of Ag nanoparticles results in an increase of depletion region and, hence, reduces the conductivity of the sensor. This result is supported by the X-ray photoelectron spectroscopy (XPS) shown in Fig. 8. At room temperature, the Ag 3-D spectrum shows a mixture state: a metallic state at 368 eV appearing at the shoulder of the Ag 3-D, and a main oxidation state signal at 367.4 eV. This indicates that at RT, the Ag is partially oxidized. While after annealing at 200 °C, the metallic signal disappears completely, leaving only a sharp oxidation state. The results indicate that annealing has increased significantly the oxidation rate of the Ag surface in the sample.

Total 26 833 sampling points are used to train, test, and validate a shallow NN with one hidden layer and ten hidden neurons. The estimation performance of the NN-based only on a single WO_3 sensor operating at 25 °C is given in Fig. 9, where the mean squared error (mse) observed is quite high and the best validation performance achieved is 8233.91 after six validation checks. As the response of the sensor while operating at 25 °C is not very sensitive toward the concentration of H_2S, the performance of the NN is also weak.

Furthermore, as the response of the sensor becomes more sensitive while operating at higher temperatures, as shown in Fig. 7, the performance of the NN model is also observed to achieve high prediction accuracy. The actual and estimated concentration values of H_2S using the response of sensor at four different temperatures (T = 25 °C, 80 °C, 150 °C, 200 °C) are shown in Fig. 10(a–d). It can be seen from the results in Fig. 10 that the model is able to estimate the concentration of gas more accurately at higher temperatures, while the performance remains weak at lower operating temperatures. Table II enlists some performance evaluation parameters for the single WO_3 sensor operating at different temperatures.

In order to further enhance the performance of the model, the response of four sensors is combined and is tested for estimation of H_2S. The performance of an array of four sensors toward the prediction of H_2S is given in detail in Section IV-B.

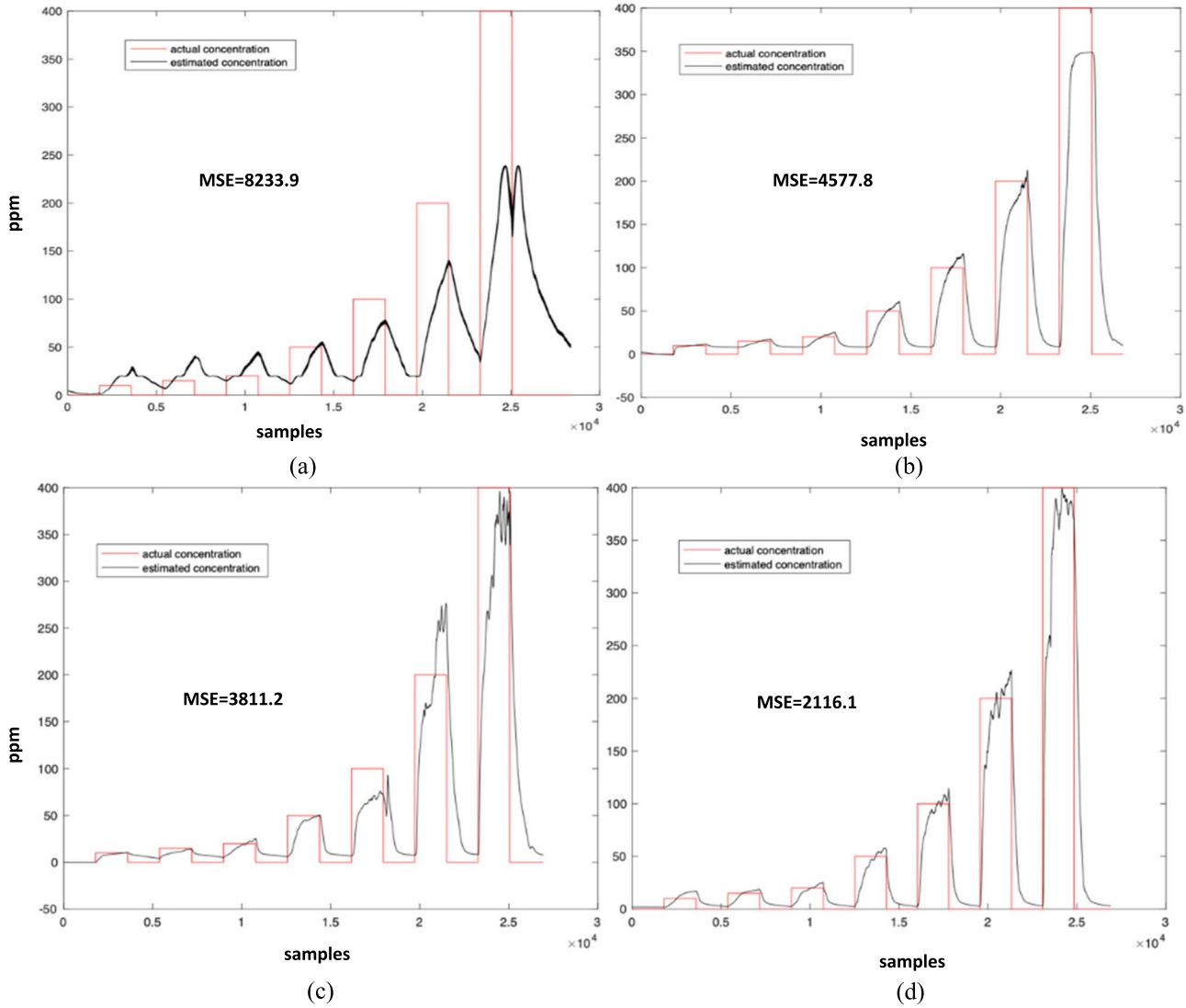

Fig. 10. Actual versus estimated concentration using a single pure WO_3 sensor response. Sensor operating at (a) 25 °C, (b) 80 °C, (c) 150 °C, and (d) 200 °C.

TABLE II
PERFORMANCE EVALUATION OF A SINGLE WO_3 SENSOR

	Performance			
Temperature	25^0C	80^0C	150^0C	200^0C
MSE	8233.9	4577.8	3811.2	2116.1
R (Validation)	0.4907	0.7688	0.8199	0.9044
R (Testing)	0.5425	0.8113	0.8230	0.8959
R (Training)	0.5015	0.8076	0.8376	0.8941
R (All Data)	0.5060	0.8025	0.8327	0.8960

TABLE III
PERFORMANCE EVALUATION OF FOUR SENSORS ARRAYS

	Performance			
Temperature	25^0C	80^0C	150^0C	200^0C
MSE	993.85	718.09	159.80	498.57
R (Validation)	0.9512	0.9670	0.9930	0.9773
R (Testing)	0.9562	0.9720	0.9930	0.9788
R (Training)	0.9582	0.9651	0.9924	0.9796
R (All Data)	0.9569	0.9665	0.9926	0.9791

B. Performance of Four Sensors Array Operating at Different Temperatures

The prediction performance of the sensors array is shown in Fig. 11, where the concentration of H_2S is estimated using the sensors array operating at four different temperatures. From the prediction results, it can be seen that there is a significant improvement as compared with the results of a single sensor operating at the same temperatures, specifically at 25 °C. This shows that an array of different sensors has a powerful discriminatory power as compared with a single sensor operating at lower temperatures. However, a comparable performance is observed at higher operating temperatures. Table III enlists the performance evaluation parameters for the array of sensors operating at four different temperatures.

C. Performance of FDFs

FDFs are proposed as a new set of features for the estimation of the concentration of gases. The performance of the proposed features extracted from the response of a single sensor is shown in Fig. 12. It can be seen from the

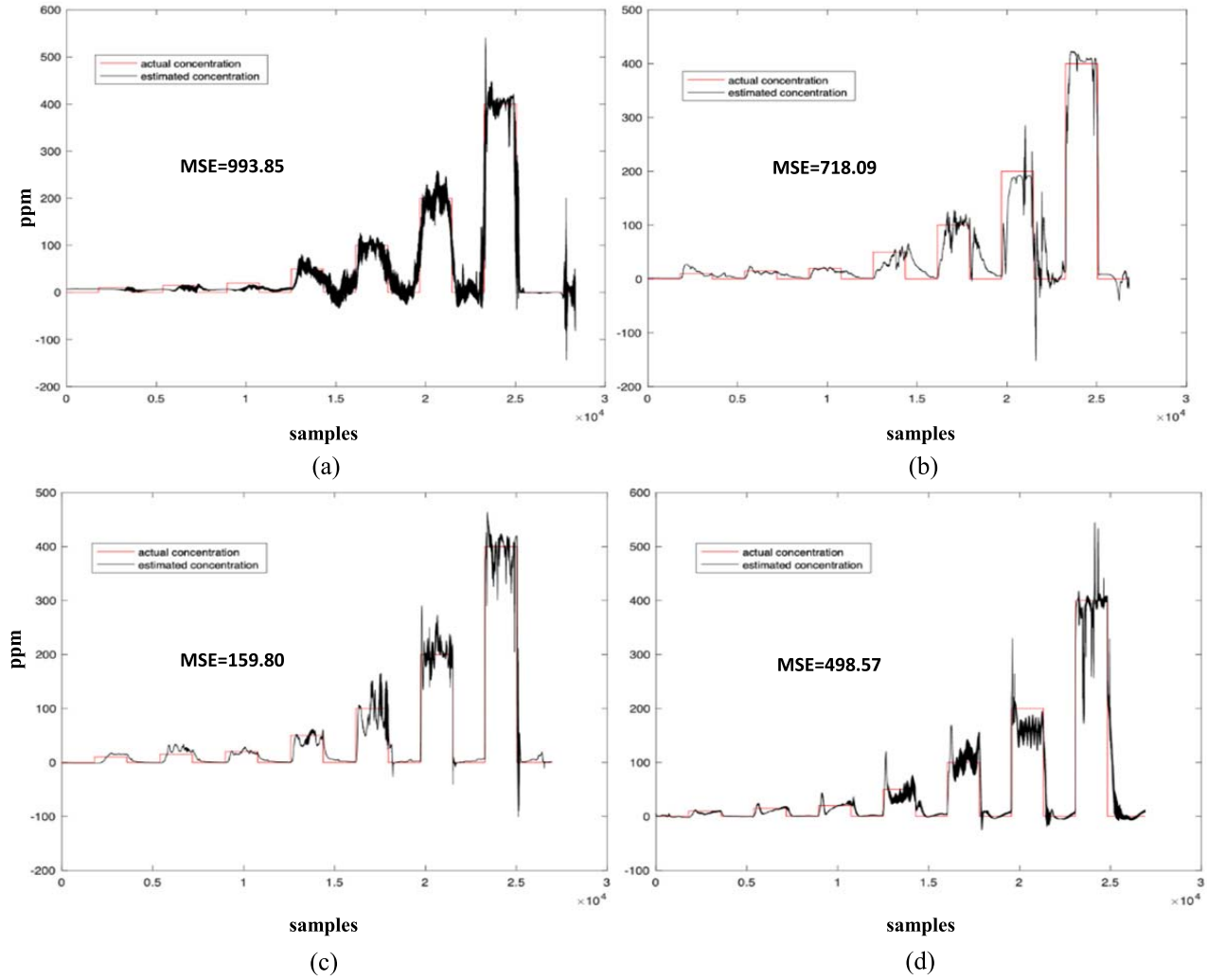

Fig. 11. Actual versus estimated concentration using an array of four sensors. Sensor operating at (a) 25 °C, (b) 80 °C, (c) 150 °C, and (d) 200 °C.

TABLE IV
PERFORMANCE EVALUATION WITH FDF OF A SINGLE SENSOR

	Performance			
Temperature	25^0C	80^0C	150^0C	200^0C
MSE	644.50	470.78	746.44	258.50
R (Validation)	0.9686	0.9780	0.9659	0.9888
R (Testing)	0.8799	0.9841	0.9643	0.9890
R (Training)	0.9681	0.9847	0.9661	0.9876
R (All Data)	0.9541	0.9837	0.9658	0.9880

TABLE V
PERFORMANCE EVALUATION WITH FDF OF FOUR SENSORS ARRAY

	Performance			
Temperature	25^0C	80^0C	150^0C	200^0C
MSE	286.13	74.90	8.99	18.23
R (Validation)	0.9866	0.9968	0.9996	0.9991
R (Testing)	0.9875	0.9960	0.9994	0.9992
R (Training)	0.9877	0.9965	0.9996	0.9994
R (All Data)	0.9875	0.9964	0.9995	0.9993

estimation results reported in Fig. 12 that the proposed features are powerful enough to estimate the concentration of H_2S using only a single sensor operating at 25 °C. However, the estimation of low concentration values is not as good as the estimation of higher concentration values. The results shown in Fig. 12 clearly demonstrate the ability of proposed features to estimate the concentration of H_2S. Table IV enlists the performance evaluation parameters of FDFs extracted from a single sensor response, operating at different temperatures.

Furthermore, to make the feature vector stronger toward the estimation of gas, the features extracted from the response of the sensors array is also used. The results of features extracted from the response of array of four sensors operating at different temperatures are shown in Fig. 13. The visual results depicted in Fig. 13 further strengthen the concept of employing fractional derivate features for the estimation of H_2S as the performance is greatly improved at all operating temperatures, specifically at 25 °C. Table V enlists the performance evaluation parameters of FDF extracted from an array of sensors responses operating at different temperatures.

D. Performance of Virtual Sensors Array

When four physical sensors are operated at four different temperatures, a maximum of 16 virtual sensors array is created. The 16-channel response of this virtual sensors array is

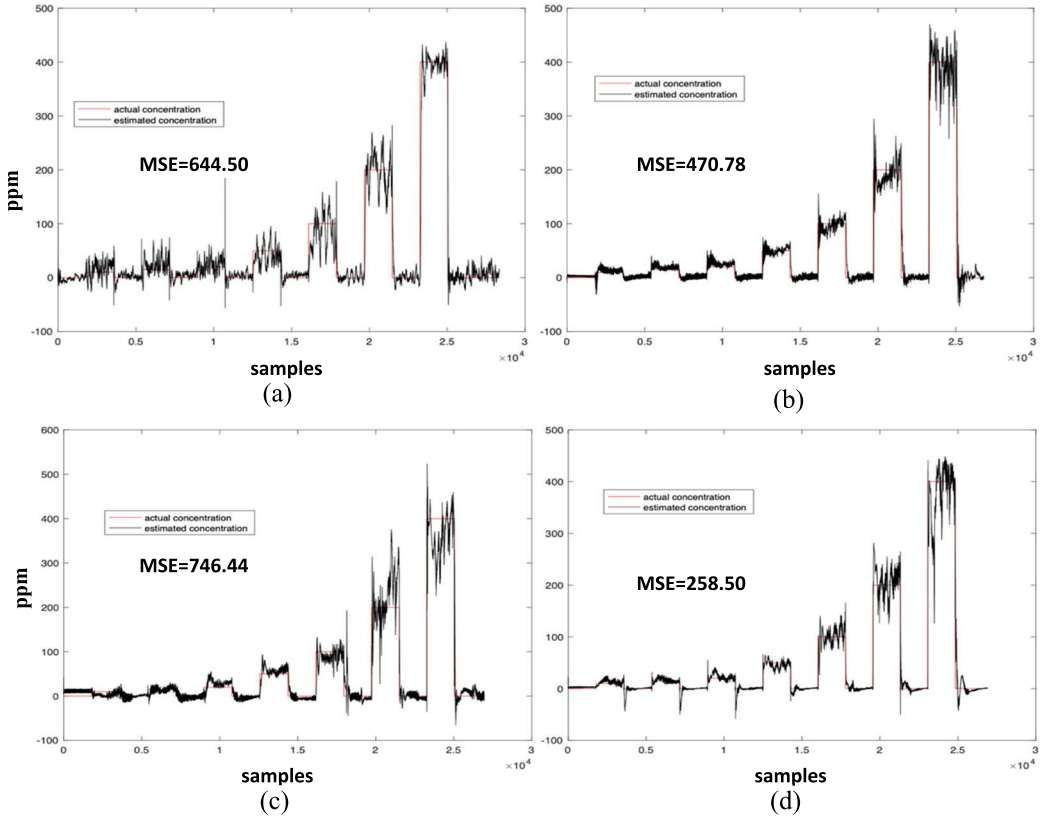

Fig. 12. Actual versus estimated concentration using fractional derivative computed from a single sensor response. Sensor operating at (a) 25 °C, (b) 80 °C, (c) 150 °C, and (d) 200 °C.

TABLE VI
PERFORMANCE EVALUATION OF VIRTUAL SENSORS ARRAY

Performance	2 virtual sensors	4 virtual sensors	8 virtual sensors	12 virtual sensors	16 virtual sensors	FDF of 16 virtual sensors
No. of sensors	1	1	2	3	4	4
Sensor Type(s)	WO_3	WO_3	WO_3, and $WO_3@_{1\%Ag}$	WO_3, $WO_3@_{1\%Ag}$, and $WO_3@_{3\%Ag}$	WO_3, $WO_3@_{1\%Ag}$, $WO_3@_{3\%Ag}$, and $WO_3@_{5\%Ag}$	WO_3, $WO_3@_{1\%Ag}$, $WO_3@_{3\%Ag}$, and $WO_3@_{5\%Ag}$
Operating temperatures	25^0C, 80^0C	25^0C, 80^0C, 150^0C, 200^0C	25^0C, 80^0C, 150^0C, 200^0C	25^0C, 80^0C, 150^0C, 200^0C	25^0C, 80^0C, 150^0C, 200^0C	25^0C, 80^0C, 150^0C, 200^0C
MSE	1759.86	31.21	8.33	6.31	4.61	**0.9076**
R (Validation)	0.9060	0.9984	0.9996	0.9997	0.9997	**0.9999**
R (Testing)	0.9101	0.9985	0.9996	0.9997	0.9997	**0.9999**
R (Training)	0.8947	0.9985	0.9996	0.9997	0.9997	**0.9999**
R (All)	0.8988	0.9985	0.9996	0.9997	0.9997	**0.9999**

recorded and analyzed for estimation of H_2S in air samples. The estimation results of this 16 virtual sensors array are shown in Fig. 14. The estimation results using the concept of virtual sensing are the most promising results as the concept has clearly demonstrated the highly accurate estimation of H_2S. However, to practically implement the concept, an operation of sensors at high temperatures is required, whereas a good estimation is also possible using the newly proposed FDF concept and operating the sensors at 25 °C. Table VI enlists the performance evaluation of virtual sensing arrays with different lengths and the performance evaluation of virtual sensing with associated FDF. From the results reported in Table VI, it can be seen that with an increase in the amount of virtual sensors, the estimation accuracy of H_2S is increased. This shows that the variation in sensors response caused by different operating temperatures can result in unique signatures for different

TABLE VII
PERFORMANCE COMPARISON

Performance	PCA Virtual array	LDA Virtual array	FDF Virtual array
MSE	5.0366	11.6089	**0.9076**
R (Validation)	0.9997	0.9994	**0.9999**
R (Testing)	0.9997	0.9994	**0.9999**
R (Training)	0.9997	0.9995	**0.9999**
R (All)	0.9997	0.9995	**0.9999**

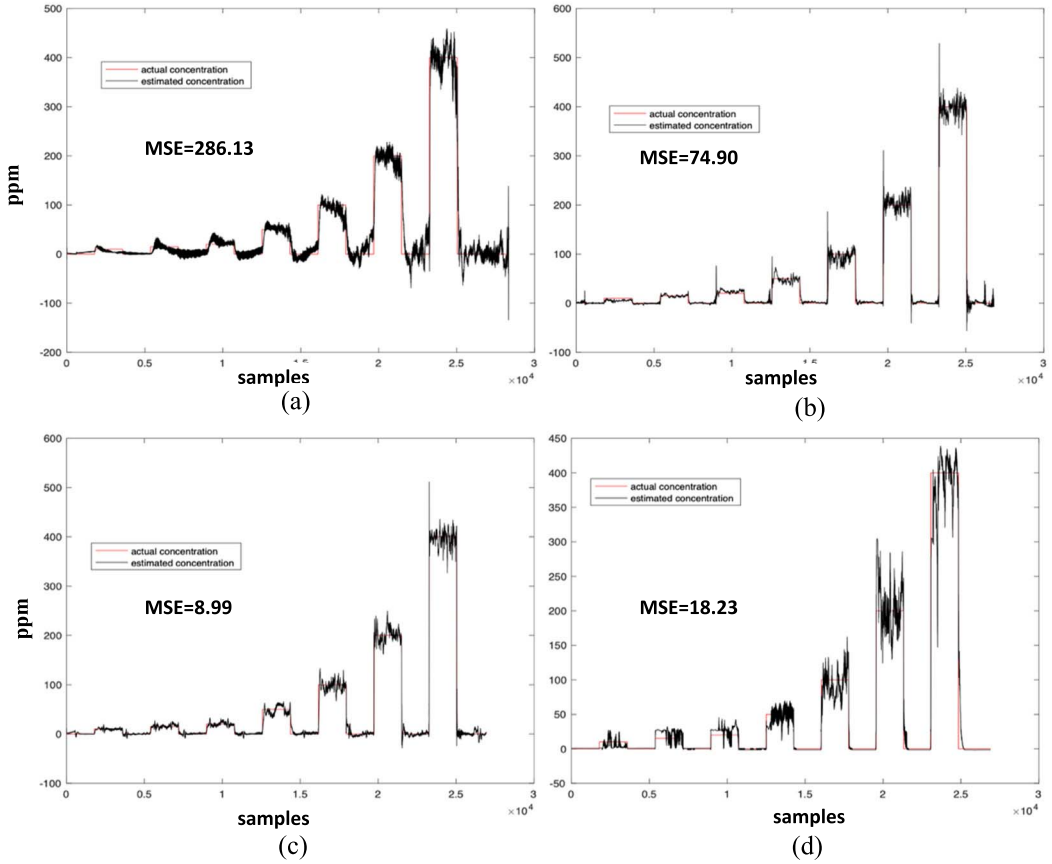

Fig. 13. Actual versus estimated concentration using fractional derivative computed from sensors array response. Sensor operating at (a) 25 °C, (b) 80 °C, (c) 150 °C, and (d) 200 °C.

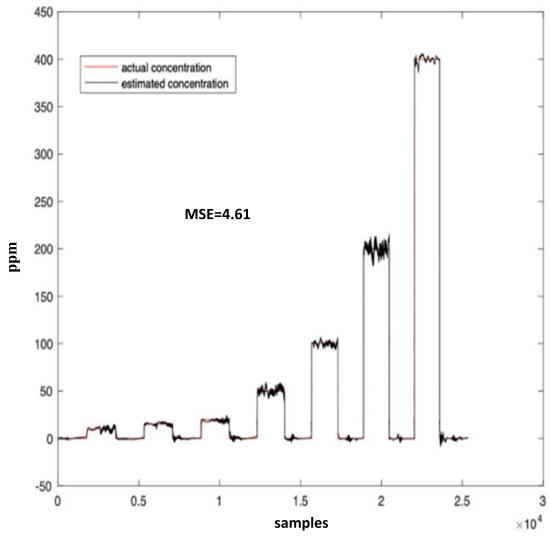

Fig. 14. Estimation using the concept of virtual sensing: combined response of four different sensors operating at four different temperatures.

concentration levels of H_2S. Thus, more variations recorded result in more accurate estimation. Furthermore, it can also be seen that the addition of FDF further enhances the estimation performance of the proposed system.

In order to better realize the effectiveness of the proposed FDF features, the performance comparison results with the two most commonly used state-of-the-art methods PCA and LDA are provided in Table VII. The two types of feature extraction methods are used to extract features from the virtual sensing array and the results are compared with the proposed FDF features extracted from the same virtual sensing array. From the results in Table VII, it is clearly seen that the proposed FDF features contain powerful discriminatory information as compared with the PCA and the LDA.

V. Conclusion

A highly precise and robust system to estimate the concentration of H_2S in air samples is proposed. The proposed system is based on a *virtual sensing* concept that employs WO_3 sensors developed in the in-house foundry and a shallow NN model enhanced with FDFs. The mse value for estimation of H_2S dropped from 159.80 [best performance in case of four physical sensors array operating at 1500C (see Table III)] to 4.61 [in case of 16 virtual sensors array (see Table VI)]. The use of FDF along with virtual sensors array further decreased the mse value to 0.9076, resulting in best performance for estimation of H_2S in air samples. However, to implement the concept demonstrated by virtual sensing in real scenarios, it requires an operation of sensors at higher temperatures. Contrary to the virtual sensing concept, the newly proposed feature extraction technique called FDF also resulted in high precision estimation of H_2S with sensors operating at 25 °C. Therefore, features derived from fractional derivatives are

highly recommended for scenarios where the operation of sensors at high temperatures is not feasible, whereas the results drawn from virtual sensing provide a strong recommendation to use a combined response of different sensors operating at different temperatures to estimate the concentration of H_2S in scenarios where the operation of sensors at higher temperatures is feasible.

ACKNOWLEDGMENT

The publication of this article was funded by the Qatar National Library. The findings herein reflect the work and are solely the responsibility of the authors.

REFERENCES

[1] S. L. M. Rubright, L. L. Pearce, and J. Peterson, "Environmental toxicology of hydrogen sulfide," *Nitric Oxide*, vol. 71, pp. 1–13, Dec. 2017.

[2] B. Chou *et al.*, *Division of Toxicology and Environmental Medicine/Applied Toxicology Branch* (Toxicological Profile for Hydrogen Sulfide and Carbonyl Sulfide). Atlanta, GA, USA: US Department of Health and Human Services, 2016.

[3] R. Thompson, J. D. Perry, S. P. Stanforth, and J. R. Dean, "Rapid detection of hydrogen sulfide produced by pathogenic bacteria in focused growth media using SHS-MCC-GC-IMS," *Microchem. J.*, vol. 140, pp. 232–240, Jul. 2018.

[4] D.-Y. Lee, W.-C. Huang, T.-J. Gu, and G.-D. Chang, "Quantitative and comparative liquid chromatography-electrospray ionization-mass spectrometry analyses of hydrogen sulfide and thiol metabolites derivaitized with 2-iodoacetanilide isotopologues," *J. Chromatogr. A*, vol. 1552, pp. 43–52, Jun. 2018.

[5] S. K. Pandey and K.-H. Kim, "A review of methods for the determination of reduced sulfur compounds (RSCs) in air," *Environ. Sci. Technol.*, vol. 43, no. 9, pp. 3020–3029, May 2009.

[6] S. K. Pandey, K.-H. Kim, and K.-T. Tang, "A review of sensor-based methods for monitoring hydrogen sulfide," *Trends Anal. Chem.*, vol. 32, pp. 87–99, Feb. 2012.

[7] M. Asif *et al.*, "Hierarchical CNTs@CuMn layered double hydroxide nanohybrid with enhanced electrochemical performance in H_2S detection from live cells," *Anal. Chem.*, vol. 91, no. 6, pp. 3912–3920, 2019.

[8] I. Urriza-Arsuaga, M. Bedoya, and G. Orellana, "Unprecedented reversible real-time luminescent sensing of H_2S in the gas phase," *Anal. Chem.*, vol. 91, no. 3, pp. 2231–2238, 2019.

[9] R. Kaushik, R. Sakla, A. Ghosh, G. T. Selvan, P. M. Selvakumar, and D. A. Jose, "Selective detection of H_2S by copper complex embedded in vesicles through metal indicator displacement approach," *ACS Sensors*, vol. 3, no. 6, pp. 1142–1148, Jun. 2018.

[10] Y. Zhang, H.-Y. Shen, X. Hai, X.-W. Chen, and J.-H. Wang, "Polyhedral oligomeric silsesquioxane polymer-caged silver nanoparticle as a smart colorimetric probe for the detection of hydrogen sulfide," *Anal. Chem.*, vol. 89, no. 2, pp. 1346–1352, Jan. 2017.

[11] S. K. Patra, S. K. Sheet, B. Sen, K. Aguan, D. R. Roy, and S. Khatua, "Highly sensitive bifunctional probe for colorimetric cyanide and fluorometric H_2S detection and bioimaging: Spontaneous resolution, aggregation, and multicolor fluorescence of bisulfide adduct," *J. Organic Chem.*, vol. 82, no. 19, pp. 10234–10246, Oct. 2017.

[12] C.-G. Dai, X.-L. Liu, X.-J. Du, Y. Zhang, and Q.-H. Song, "Two-input fluorescent probe for thiols and hydrogen sulfide chemosensing and live cell imaging," *ACS Sensors*, vol. 1, no. 7, pp. 888–895, Jul. 2016.

[13] L. A. Montoya and M. D. Pluth, "Organelle-targeted H_2S probes enable visualization of the subcellular distribution of H_2S donors," *Anal. Chem.*, vol. 88, no. 11, pp. 5769–5774, Jun. 2016.

[14] S. K. Bae *et al.*, "A ratiometric two-photon fluorescent probe reveals reduction in mitochondrial H_2S production in Parkinson's disease gene knockout astrocytes," *J. Amer. Chem. Soc.*, vol. 135, no. 26, pp. 9915–9923, Jul. 2013.

[15] G. Hu, Y. Li, L. Li, S. Xu, and L. Wang, "Fluorinated $ZnFe^{III}$ hollow metal–organic framework as a ^{19}F NMR probe for highly sensitive and selective detection of hydrogen sulfide," *ACS Omega*, vol. 5, no. 14, pp. 8373–8379, 2020.

[16] W. Chen, D. Ni, Z. T. Rosenkrans, T. Cao, and W. Cai, "Smart H_2S-triggered/therapeutic system (SHTS)-based nanomedicine," *Adv. Sci.*, vol. 6, no. 22, Nov. 2019, Art. no. 1901724.

[17] R. Zhang *et al.*, "Real-time discrimination and versatile profiling of spontaneous reactive oxygen species in living organisms with a single fluorescent probe," *J. Amer. Chem. Soc.*, vol. 138, no. 11, pp. 3769–3778, Mar. 2016.

[18] A. Shamirian, H. S. Afsari, D. Wu, L. W. Miller, and P. T. Snee, "Ratiometric QD-FRET sensing of aqueous H_2S *in vitro*," *Anal. Chem.*, vol. 88, no. 11, pp. 6050–6056, Jun. 2016.

[19] N. Adarsh, M. S. Krishnan, and D. Ramaiah, "Sensitive naked eye detection of hydrogen sulfide and nitric oxide by aza-BODIPY dyes in aqueous medium," *Anal. Chem.*, vol. 86, no. 18, pp. 9335–9342, Sep. 2014.

[20] S. He, J. Hai, S. Sun, S. Lu, and B. Wang, "Palladium coordination polymers nanosheets: New strategy for sensitive photothermal detection of H_2S," *Anal. Chem.*, vol. 91, no. 16, pp. 10823–10829, Aug. 2019.

[21] X. Bai, S. Xu, and L. Wang, "Full-range pH stable au-clusters in nanogel for confinement-enhanced emission and improved sulfide sensing in living cells," *Anal. Chem.*, vol. 90, no. 5, pp. 3270–3275, Mar. 2018.

[22] Z. Yuan *et al.*, "Selective colorimetric detection of hydrogen sulfide based on primary amine-active ester cross-linking of gold nanoparticles," *Anal. Chem.*, vol. 87, no. 14, pp. 7267–7273, Jul. 2015.

[23] Z. Yunusa, M. N. Hamidon, A. Kaiser, and Z. Awang, "Gas sensors: A review," *Sensore Transducers*, vol. 168, no. 4, pp. 61–75, 2014.

[24] M. Khan, M. Rao, and Q. Li, "Recent advances in electrochemical sensors for detecting toxic gases: NO_2, SO_2 and H_2S," *Sensors*, vol. 19, no. 4, p. 905, Feb. 2019.

[25] M. H. Suhail, O. G. Abdullah, and G. A. Kadhim, "Hydrogen sulfide sensors based on PANI/f-SWCNT polymer nanocomposite thin films prepared by electrochemical polymerization," *J. Sci., Adv. Mater. Devices*, vol. 4, no. 1, pp. 143–149, Mar. 2019.

[26] Z. Yuan, E. Han, F. Meng, and K. Zuo, "Detection and identification of volatile organic compounds based on temperature-modulated ZnO sensors," *IEEE Trans. Instrum. Meas.*, vol. 69, pp. 4533–4544, 2020.

[27] Z. Li *et al.*, "Advances in designs and mechanisms of semiconducting metal oxide nanostructures for high-precision gas sensors operated at room temperature," *Mater. Horizons*, vol. 6, no. 3, pp. 470–506, 2019.

[28] B. Guo, A. Bermak, P. C. H. Chan, and G.-Z. Yan, "An integrated surface micromachined convex microhotplate structure for tin oxide gas sensor array," *IEEE Sensors J.*, vol. 7, no. 12, pp. 1720–1726, Dec. 2007.

[29] A. B. Far, F. Flitti, B. Guo, and A. Bermak, "A bio-inspired pattern recognition system for tin-oxide gas sensor applications," *IEEE Sensors J.*, vol. 9, no. 6, pp. 713–722, Jun. 2009.

[30] A. Sultangazin, J. Kusmangaliyev, A. Aitkulov, D. Akilbekova, M. Olivero, and D. Tosi, "Design of a smartphone plastic optical fiber chemical sensor for hydrogen sulfide detection," *IEEE Sensors J.*, vol. 17, no. 21, pp. 6935–6940, Nov. 2017.

[31] M. B. Banerjee *et al.*, "Development of a low-cost portable gas sensing system based on molecularly imprinted quartz crystal microbalance sensor for detection of eugenol in clove oil," *IEEE Trans. Instrum. Meas.*, vol. 70, pp. 1–10, 2021.

[32] N. X. Thai, N. Van Duy, N. D. Hoa, C. M. Hung, H. Nguyen, and N. Van Hieu, "Gas sensor array based on tin oxide nano structure for volatile organic compounds," *Vietnam J. Sci. Technol.*, vol. 58, no. 2, pp. 189–196, 2020.

[33] J. Chen *et al.*, "Ultra-low-power smart electronic nose system based on three-dimensional tin oxide nanotube arrays," *ACS Nano*, vol. 12, no. 6, pp. 6079–6088, Jun. 2018.

[34] A. Mirzaei, S. S. Kim, and H. W. Kim, "Resistance-based H_2S gas sensors using metal oxide nanostructures: A review of recent advances," *J. Hazardous Mater.*, vol. 357, pp. 314–331, Sep. 2018.

[35] F. I. M. Ali, F. Awwad, Y. E. Greish, and S. T. Mahmoud, "Hydrogen sulfide (H_2S) gas sensor: A review," *IEEE Sensors J.*, vol. 19, no. 7, pp. 2394–2407, Apr. 2019.

[36] H. Yu, H. Yu, J. Li, Y. Tian, and Z. Li, "Gas sensing and electrochemical behaviors of Ag-doped 3D spherical WO_3 assembled by nanostrips to formaldehyde," *Int. J. Electrochem. Sci.*, vol. 13, no. 10, pp. 9281–9291, Oct. 2018.

[37] L. Chen and S. C. Tsang, "Ag doped WO_3-based powder sensor for the detection of NO gas in air," *Sens. Actuators B, Chem.*, vol. 89, nos. 1–2, pp. 68–75, Mar. 2003.

[38] R. Malik, V. Chaudhary, V. K. Tomer, and S. P. Nehra, "Nanocasted synthesis of Ag/WO_3 nanocomposite with enhanced sensing and photocatalysis applications," *Energy Environ. Focus*, vol. 6, no. 1, pp. 43–48, Mar. 2017.

[39] S. Feng *et al.*, "Review on smart gas sensing technology," *Sensors*, vol. 19, no. 17, p. 3760, Aug. 2019.

[40] A. U. Rehman and A. Bermak, "Drift-insensitive features for learning artificial olfaction in E-nose system," *IEEE Sensors J.*, vol. 18, no. 17, pp. 7173–7182, Sep. 2018.
[41] A. U. Rehman and A. Bermak, "Heuristic random forests (HRF) for drift compensation in electronic nose applications," *IEEE Sensors J.*, vol. 19, no. 4, pp. 1443–1453, Feb. 2019.
[42] M. A. H. Khan, A. Motayed, and M. V. Rao, "Identification and quantification of gases and their mixtures using GaN sensor array and artificial neural network," *Meas. Sci. Technol.*, vol. 32, no. 5, May 2021, Art. no. 055111.
[43] A. U. Rehman, S. B. Belhaouari, M. Ijaz, A. Bermak, and M. Hamdi, "Multi-classifier tree with transient features for drift compensation in electronic nose," *IEEE Sensors J.*, vol. 21, no. 5, pp. 6564–6574, Mar. 2021.
[44] A. U. Rehman and A. Bermak, "Discriminant analysis of industrial gases for electronic nose applications," in *Proc. IEEE Int. Conf. Comput. Intell. Virtual Environ. Meas. Syst. Appl. (CIVEMSA)*, Jun. 2018, pp. 1–5.
[45] A. U. Rehman, A. Bermak, and M. Hamdi, "Shuffled frog-leaping and weighted cosine similarity for drift correction in gas sensors," *IEEE Sensors J.*, vol. 19, no. 24, pp. 12126–12136, Dec. 2019.
[46] A. ur Rehman and A. Bermak, "Concentration estimation of industrial gases for electronic nose applications," in *Proc. 30th Int. Conf. Microelectron. (ICM)*, Dec. 2018, pp. 13–16.
[47] M. A. Akbar *et al.*, "An empirical study for PCA- and LDA-based feature reduction for gas identification," *IEEE Sensors J.*, vol. 16, no. 14, pp. 5734–5746, Jul. 2016.
[48] S. Brahim-Belhouari, A. Bermak, M. Shi, and P. C. H. Chan, "Fast and robust gas identification system using an integrated gas sensor technology and Gaussian mixture models," *IEEE Sensors J.*, vol. 5, no. 6, pp. 1433–1444, Dec. 2005.
[49] A. ur Rehman and A. Bermak, "Recursive DBPSO for computationally efficient electronic nose system," *IEEE Sensors J.*, vol. 18, no. 1, pp. 320–327, Jan. 2018.
[50] A. Bermak and S. B. Belhouari, "Bayesian learning using Gaussian process for gas identification," *IEEE Trans. Instrum. Meas.*, vol. 55, no. 3, pp. 787–792, Jun. 2006.
[51] K. S. Miller and B. Ross, *An Introduction to the Fractional Calculus and Fractional Differential Equations*. Hoboken, NJ, USA: Wiley, 1993, p. 366.
[52] I. Petras, "Fractional derivatives, fractional integrals, and fractional differential equations in MATLAB," in *Engineering Education and Research Using MATLAB*. London, U.K.: InTech, 2011.
[53] Jonathan. (2021). *Fractional Derivative*. Accessed: Feb. 8, 2021. [Online]. Available: https://www.mathworks.com/matlabcentral/fileexchange/45982-fractional-derivative

Ahmed Alsarraj received the master's degree in engineering management from Qatar University, Doha, Qatar, in 2015. He is currently pursuing the Ph.D. degree in sustainable energy with Hamad Bin Khalifa University, Ar-Rayyan, Qatar.

He is currently working as a Student Researcher with the College of Science and Engineering, Hamad Bin Khalifa University. His research interests include gas sensors of volatile organic compounds from material and electrodes design to analysis and improvement of response.

Atiq Ur Rehman (Member, IEEE) received the master's degree in computer engineering from the National University of Sciences and Technology (NUST), Islamabad, Pakistan, in 2013, and the Ph.D. degree in computer science and engineering from Hamad Bin Khalifa University, Ar-Rayyan, Qatar, in 2019.

He is currently working as a Post-Doctoral Researcher with the College of Science and Engineering, Hamad Bin Khalifa University. His research interests include the development of evolutionary computation, pattern recognition, and machine learning algorithms.

Samir Brahim Belhaouari (Senior Member, IEEE) received the master's degree in telecommunications from the National Polytechnic Institute (ENSEEIHT) of Toulouse, Toulouse, France, in 2000, and the Ph.D. degree in applied mathematics from the Federal Polytechnic School of Lausanne (EPFL), Lausanne, Switzerland, in 2006.

He is currently an Associate Professor with the Division of Information and Computing Technology, College of Science and Engineering, Hamad Bin Khalifa University (HBKU), Ar-Rayyan, Qatar. He also holds and leads several academic and administrator positions, such as the Vice Dean of Academic and Student Affairs at the College of Science and General Studies and the University Preparatory Program at Alfaisal University, Riyadh, Saudi Arabia; University of Sharjah, Sharjah, United Arab Emirates; Innopolis University, Innopolis, Russia; Universiti Teknologi PETRONAS, Seri Iskandar, Malaysia; and EPFL Federal Swiss School, Lausanne. He is currently working actively on developing algorithms in machine learning applied to visual surveillance, sensing technologies, and biomedical data, with the support of several international funds for research in Russia, Malaysia, and in Gulf Cooperation Council (GCC). His main research interests include stochastic processes, machine learning, and number theory.

Khaled M. Saoud received the B.Sc. degree from Yarmouk University, Irbid, Jordan, in 1990, and the M.S. degree in applied physics and the Ph.D. degree in chemical physics from Virginia Commonwealth University, Richmond, VA, USA, in 2000 and 2008, respectively.

He is a Professor of physics at Liberal Arts and Sciences Program, Virginia Commonwealth University in Qatar (VCUArts-Qatar), Doha, Qatar. He also serves on two international journals' editorial boards and a reviewer of over 15 peer-reviewed journals. He has over 22 years of research, industrial, and teaching experience, including his previous positions at major American companies such as Philip Morris USA, Intel Corporation, and Nova Measuring Instruments Inc. He holds three U.S. patents and was the Lead Principal Investigator on a recent patent titled "Methods of Forming Aerogels." He has published over 53 refereed papers and book chapters and delivered over 40 keynotes, talks, and conference presentations. His research was featured more than 16 times in local and international media. His current research is focused on developing new nanostructured materials for environmental nanocatalysts, 3-D printing, nanotextiles, nanosensors, photocatalysts for wastewater treatment, and anti-bacterial and antiviral surface coating.

Dr. Saoud was a recipient of several awards, including the Challenge 22 Award for designing a Sustainable Material for World Cup 2022, the Nanotech Dubai 2015 Distinguished Scientist Award, Virginia Commonwealth University in Qatar Faculty Achievement Award in Research, Qatar Annual Research Conference (ARC13) Health Research Posters Award, Virginia Commonwealth University in Qatar Faculty Achievement Award in Teaching, and Philip Morris USA Ph.D. Research Award Grant.

Amine Bermak (Fellow, IEEE) received the M.Eng. and Ph.D. degrees in electronic engineering from Paul Sabatier University, Toulouse, France, in 1994 and 1998, respectively.

He was with the French National Research Center, Microsystems and Microstructures Research Group, Laboratory for Analysis and Architecture of Systems/Centre National de la Recherche Scientifique (LAAS-CNRS), where he developed a 3-D very large-scale integration (VLSI) chip for artificial neural network classification and detection applications. He joined the Advanced Computer Architecture Research Group, York University, York, U.K., where he held a post-doctoral position on VLSI implementation of correlation matrix memory (CMM) neural network for vision applications in a project funded by the British Aerospace. In 1998, he joined Edith Cowan University, Perth, WA, Australia, as a Research Fellow in smart vision sensors, and a Senior Lecturer with the School of Engineering and Mathematics. He was a Professor with the Electronic and Computer Engineering Department, The Hong Kong University of Science and Technology, Hong Kong, where he was also serving as the Director of Computer Engineering and the Director of the M.Sc. degree Program in integrated circuit design. He is currently a Professor and an Associate Dean at the College of Science and Engineering, Hamad Bin Khalifa University, Ar-Rayyan, Qatar. His research interests include VLSI circuits and systems for signal, image processing, sensors, and microsystem applications.